A LOW TEMPERATURE AQUEOUS SOLUTION PROCESSING ROUTE FOR IGZO THIN FILMS EMPLOYING ELECTROCHEMICALLY SYNTHESIZED InGaZn CLUSTERS

by

MAHKAH ZHAN-WEI BUSSELL WU

A THESIS

Presented to the Department of Chemistry
and the Robert D. Clark Honors College
in partial fulfillment of the requirements for the degree of
Bachelor of Science

June 2014

An Abstract of the Thesis of

Mahkah Z. B. Wu for the degree of Bachelor of Science
in the Department of Chemistry to be taken June 2014

Title: A Low Temperature Aqueous Solution Processing Route for IGZO Thin Films
Employing Electrochemically Synthesized InGaZn Clusters

Approved: _____

Shannon W. Boettcher

Owing to the growth of its applications, including solar cells, electrochromatic windows, and especially active channel layers in thin film transistors (TFTs), amorphous indium gallium zinc oxide (IGZO) has become an area of significant research interest. In particular, a low temperature solution based fabrication route for IGZO would enable greater application as it would decrease manufacturing costs, enable large area deposition, and make IGZO compatible with low temperature substrates. Here, a previously unreported nanocluster was synthesized in solution. In addition to characterizing the solution with dynamic light scattering, it was used as an inorganic aqueous precursor for solution deposition of IGZO thin film. Scanning electron microscopy and X-ray reflectometry revealed that films were dense and that solution precursors had sufficient metal concentration to yield films up to 15 nm thick per layer. Quartz crystal microbalance analysis and infrared transmittance spectroscopy revealed that processing temperatures of 200-250°C were sufficient to remove counter ions from the film, a significant improvement over existing sol-gel routes that necessitate the removal of organic ligands. Finally, TFT devices that were fabricated using IGZO as the active channel layer displayed high performance. In particular, a composition of In:Ga:Zn=69:12:19 yielded an average channel mobility of 15.2 $cm^2V^{-1}s^{-1}$, a turn-on voltage of ~-40 V, and an on/off current ratio of $>10^6$.

Acknowledgements

I would like to thank Dr. Shannon Boettcher for welcoming me into his lab and enabling me to do research over the previous summer. I am grateful that he has taken the time to show me just how much information can be extracted from a single piece of data, given me agency to explore projects that I have been interested in, and provided me with salient advice on what to do once I leave his lab.

Next, I would like to recognize Dr. Athavan Nadarajah for all of his help and guidance in the laboratory. When I arrived at the Boettcher Lab, Athavan was the first group member to speak to me about his research, and I am grateful that he took the time to help me learn the basics of solution processing while I worked with ZnO. Since I began working with him directly, Athavan has taught me a myriad of laboratory techniques and concepts all the while being patient with my inability to remember to remove the nickel filter from the diffractometer.

The final member of my committee, Professor Joseph Fracchia, put my college career on the correct path by underlining the dangers of cynicism and showing me the value of developing relationships with my professors. His courses are fascinating and delightfully over ambitious surveys of broad spans of history and discipline that remind of the value of being interested in everything. Perhaps without even knowing it, Professor Fracchia has caused me to take on some of the most ambitious challenges of

my college career, including suggesting that I speak to Shannon and putting in a good word for me with distinguished scholarship advisers.

Beyond my committee, I would like to thank the members of the Boettcher Lab for making me feel like a valued group member. In particular, Matt Kast guided me through my first project on ZnO and gladly let me snare him in help loops whenever I needed it. Both Michela Burke and Adam "Atom" Smith have been incredibly helpful and delightful to be around. I had a great time working with Julija Vickenvitie, and she was a shining role model of an undergraduate passionate about science. In the wider Center for Sustainable Materials Chemistry, both Dr. Paul Messler and Dr. Matt Carnes have been incredibly helpful over the course of this project.

Certainly, I would not have made it through this process without my friends, Mika Weinstein and Coleman Boyer. Their contributions have ranged from mental stimulation to emotional support to literal physical nourishment.

Finally, I would like to thank my parents, Dana Bussell and Peter Wu. I am grateful for the trust and respect that they have shown for me in letting me find my own path through life. Thank you for opening doors for my study of science and your support of my desire to also study everything else.

Table of Contents

List of Figures

List of Tables

1. General Introduction

In order to appeal to a wider range of audiences, this thesis contains both a general introduction and a technical introduction. As a result, there is some redundancy between these two sections, but each take a different approach to introducing the topic. In addition, there is an appendix containing supplementary explanations of theory and laboratory techniques whose content is referenced at relevant points throughout the thesis.

1.1. Preliminaries

Owing to decades of application to nearly every form of digital technology, semiconductor materials have been so well researched that the complexity and speed of semiconductor devices has increased exponentially, a phenomenon known as Moore's Law.

Semiconductors are materials that conduct electricity more readily than insulators, such as silica glass, but not as readily as conductors, such as metals. The theory underpinning conductivity makes use of quantum mechanics to describe the behavior of charge carriers, most commonly electrons, in a material. A relevant portion of this theory is discussed in Appendix Band Theory and Electrical Properties6.1, but roughly there exist two different bands in a material, the valence and conducting bands. Most of the electrons reside in the lower energy valence band, meaning that they are associated with the valence shells of particular atoms and thus cannot freely move about the material. On the other hand, electrons in the conducting band are in the mobile phase and may freely travel about the material, generating electrical current. The energy

required to promote electrons from the valence to the conducting band is referred to as the band gap and dictates the classification of the material: metals have a band gap of zero, semiconductors have small band gaps that electrons can be thermally excited across, and insulators have large band gaps.

The small band gap of semiconductors grants them a number of important properties. For instance, their electrical properties are highly tunable via substituting impurities, a process known as doping. Depending on the material substituted, doping can increase the number of electrons or the number of holes, the other charge carrier, in the conduction band to form an n-type or p-type material, respectively. When an n-type material and a p-type material are placed next to each other, they form a diode which passes current more easily in one direction than the other. Alternatively, a material can have multiple localized p- and n-type regions, leading to variable resistance across the material or other interesting electrical properties. Finally, radiation and light have sufficient energy to promote electrons to the conducting band, making semiconductors sensitive to temperature and light. Unlike metals, the conductivity of semiconductors increases with temperature because thermal energy promotes more electrons into the conducting band. These properties lend themselves to a myriad of applications including transistors, light emitting diodes, solar panels, quantum dots, and digital and analog integrated circuits, making semiconductors foundational to nearly all electronics.

Because research into these materials is well established, current research efforts often center on semiconductors with exotic properties. Transparent conducting oxides (TCOs) are one such example. These materials are a unique class of semiconductors characterized by electrical conductivity, visible light transparency, and infrared

reflectivity.[1] Once again, the band gap plays an important role in these properties. The energy associated with a photon may be expressed as a function of the wavelength

$$E = \frac{hc}{\lambda} \tag{1}$$

The wavelength of visible light ranges from 390 to 700 nm, so according to Equation (**1**, the energy of a photon of visible light ranges from 1.77 to 3.18 eV. In order to effectively transmit visible light, TCOs cannot have a band gap within this range because they would absorb the light by promoting electrons from the valence to the conducting band (as solar cells do), rather than transmit it. As a result, TCOs generally have a wide band gap of greater than 3 eV.[2] To compensate for a wide band gap, TCOs are often doped to increase their carrier concentration and thus their conductivity.

This thesis centers on the synthesis of one such TCO, amorphous indium gallium zinc oxide (IGZO). A new synthetic processing route for IGZO was explored and the properties of the resulting material were explored using a variety of characterization techniques.

1.2. Applications

Although transparency and conductivity don't seem like complimentary properties, several applications require both. Solar panels build up charge on the side of the panel facing the sun, and a TCO enables the charge to be gathered without obstructing incident light. Similarly, in a liquid crystal display (LCD) screen, electricity must be delivered to liquid crystals without preventing the viewer from seeing them. Some applications only make use of the optical properties of TCOs; for instance, when TCOs are coated on windows, their infrared reflectance acts as thermal insulation while their visible light transparency allows the window to continue to function as a window.

Other applications include light-emitting diodes (LEDs), electrochromics, low-emissivity windows, and flexible electronics.[3–7]

Many semiconductors are crystalline, meaning that the long term structure can be abbreviated as a unit cell that is replicated over and over again. The regular structure of crystalline materials gives electrons long range paths to travel through the material, facilitating conductivity. However, these paths are highly sensitive to defects, a challenge for synthesis. Even if films are 99.999999% pure, a molar quantity of this film will contain on the order of 10^{15} impurities. To combat this, known impurities are often intentionally introduced via doping in high concentrations to overwhelm the effect of random impurities present in significantly smaller quantities.

Alternatively, amorphous materials can maintain strong electronic properties over large areas because these properties are not dependent on a uniform lattice as they are in crystalline materials. This means that these materials are well suited for application in a new area referred to as 'giant microelectronics'. The most common devices within this designation are solar cells and active-matrix (AM) flat panel displays. The principal application of IGZO is in the latter; the material's electron mobility (see Appendix 6.1.2), controllable carrier concentration (see Appendix 6.1.2), stable TFT characteristics (see Appendix 6.1.3), and scalable processing routes make it nearly ideal for these applications.[8] Utilizing IGZO, LG Electronics reported the first AM organic light emitting diode (OLED) display in 2006,[9] and Samsung Group responded in 2009 by fabricating a 12.1 inch AM-OLED, the largest at the time.[10] These applications require electron mobilities $> 4 \text{ cm}^2\text{V}^{-1}\text{S}^{-1}$, so the mobilities of existing IGZO TFTs ($> 10 \text{ cm}^2\text{V}^{-1}\text{S}^{-1}$) are sufficiently large.[8] Thus, present research into

4

IGZO has centered on improving other aspects of the material; this project fits into this framework by attempting to find a better fabrication route for IGZO by exploring aqueous precursors for solution processing. A description of solution processing and other synthetic techniques may be found in Appendix 6.2.

1.3. Clusters: Novel Aqueous Precursors

Although generating an aqueous precursor may seem as simple as dissolving metal cations in water, these solutions will crystalize too rapidly upon solvent removal, generating rough films. Aqueous inorganic nanoclusters—intermediaries between solvated ions and precipitates—are promising alternatives.[11–18] Of particular note for this thesis, so called Group 13 clusters composed of Ga_{13} and $Ga_{13-x}In_xO_y$ stabilized by hydroxo and nitro ligands, shown in Figure 1, are being explored as precursors for thin film manufacture.[19]
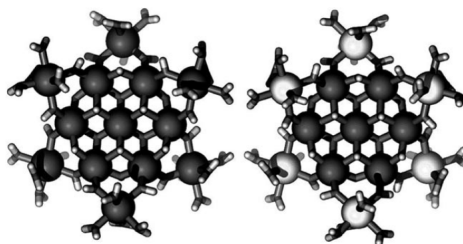
Figure 1. Structure of Ga_{13} and Ga_7In_6 nanoclusters.[19]

The molecular structures, determined by single crystal X-Ray diffraction of $[Ga_{13}(\mu_3\text{-}OH)_6(\mu\text{-}OH)_{18}(H_2O)_{24}(NO_3)_{15}]$ (left) and $[Ga_7In_6(\mu_3\text{-}OH)_6(\mu\text{-}OH)_{18}(H_2O)_{24}(NO_3)_{15}]$ (right). Ga and In are shown as dark and light spheres, respectively; ligands are shown as sticks.

Clusters may be thought of as intermediaries between ions in solution and precipitates; they form at the interfaces between these species, as the Pourbeix diagram presented in Figure 2 illustrates.
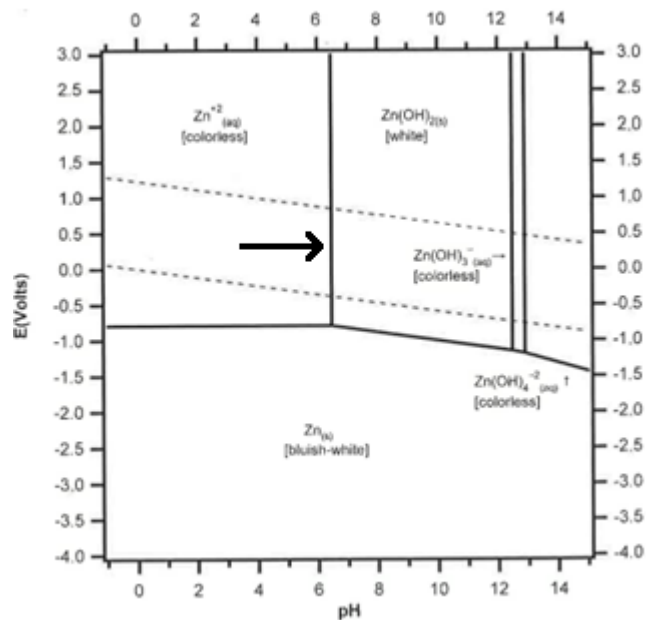
Figure 2. A Pourbeix diagram for zinc.[20]

Potential is plotted on the y-axis while pH is plotted on the x-axis. The dotted line indicates the potential range typically experienced. Each region enclosed by solid lines represents a species in solution. Cluster formation occurs when the solution approaches the interface between two regions, as indicated by the path of the arrow.

A solution may be driven to the interface by titrating with a either an acid or base, depending on the direction that must be moved along the pH axis, or by using electrochemistry. For use as precursors for thin film manufacturing, driving the pH change by applying an electrical potential is preferable because it does not introduce additional counter ions. These are problematic because they must be burned out of the film, requiring higher processing temperatures and leaving behind pores in the film. One of the primary challenges associated with using clusters is their instability; in particular, mixed metal oxide clusters are prone to precipitate from solution and must be stabilized by nitrate and hydroxide species.[21,22]

2. Technical Introduction

Transparent conducting oxides (TCOs) are typically wide band-gap (>3 eV) oxide semiconductors characterized by electrical conductivity, visible light transparency, and infrared reflectivity.[1,2] They have a variety of applications including solar cells, thin film transistors (TFTs), active-matrix (AM) flat panel displays, light-emitting diodes (LEDs), electrochromics, low-emissivity windows, and flexible electronics.[3–7]

Owing to the development of mixed metal oxide TFTs for display applications, material development for the active channel layer in TFTs has been an area of research interest. A number of TCOs, including InZnO (IZO),[23–25] SnZnO (ZTO),[26–28] and InGaZnO (IGZO),[29–33] have been explored due to their shared attributes of low processing temperature, excellent environmental stability, and high transparency, but the high carrier mobility of amorphous IGZO makes it a particularly promising material.[34]

Traditionally, MMOs have been fabricated by vacuum deposition methods including pulsed laser deposition (PLD),[29] DC magnetron sputtering,[35] and, the most widely used, RF magnetron sputtering.[8] In contrast to these methods, solution processing has been pursued as a low energy alternative. Solution processing research has overwhelmingly focused on sol-gel based methods.[32,36–38] This method is simple and inexpensive, allows the film composition to easily be adjusted, and enables a printable manufacturing process. However, the organics used to form the gel must be removed from the film via evaporation or decomposition. Generally, this necessitates annealing at temperatures of 300°C or greater in order to trigger condensation and redox

reactions as the film polymerizes/crystallizes,[28,34,39,40] and thermogravimetric analysis suggests that temperatures in excess of 500°C are needed to remove all residual organics.[36] This limits application to flexible plastic substrates[36] and leaves the film porous.[21] A more detailed description of these deposition methods may be found in Appendix 6.2.

An ideal solution precursor is characterized by the following attributes: (1) has high solubility ($\geq$1 M) in so called "green" solvents,[41] for instance water and ethanol, enabling thickness to be controlled with precursor concentration rather than number of deposition steps; (2) contains minimal counter ions and lacks organic ligands that must be driven off; (3) does not readily crystallize upon solvent removal, minimizing film roughness; (4) is stable in solution; and (5) readily cross links after spin coating to yield dense films with mild heating.[21]

Aqueous inorganic nanoscale clusters hold promise for meeting these criteria and have been explored for a diverse range of materials.[11–18] In some cases, they have demonstrated comparable properties to vacuum deposited films.[19,42–45] However, exploration of these materials has been hindered by the difficulty associated with making them. Early synthesis of Group 13 clusters utilized dibutylnitrosamine (DBNA), a known carcinogen, and required a lengthy (~2 week) evaporation and crystallization period.[14,18,19] This procedure has been improved upon for other materials, namely aluminum. For instance, gradually increasing the pH of an $Al(NO_3)_3$ solution has been reported to cause the condensation of aluminum ions into Al_{13} clusters, eliminating the need for DBNA and cutting the reaction time to two days.[46] However, this procedure employed elemental zinc to alter the pH, and the subsequently reduced species, Zn^{2+},

8

required extensive purification. Alternatively, the pH change induced using zinc can be generated electrochemically by driving the potential of the solution, and this process has been used to synthesize both flat[22] and Keggin[47] Al_{13} clusters. Electrochemical synthesis of IGZO clusters has, to the best of my knowledge, not been explored in the literature.

Here, indium gallium zinc hydroxide nitrate nanoscale clusters were electrochemically synthesized by applying a potential to drive a solution of indium, gallium, and zinc nitrate salts towards the phase boundary. These precursor solutions were deposited via spin coating, and the resulting films were characterized, compared to films made from sol-gel precursors, and used to fabricate thin film transistor (TFT) devices.

3. Experimental

Much of this work was completed working closely with postdoctoral researcher Dr. Athavan Nadarajah. I fabricated many of the films used for all experiments. However, Dr. Nadarajah performed the electrical measurements at Oregon State University while I conducted XRR experiments. For the remaining characterization techniques (DLS, SEM, QCM, IR), we worked together to carry out experiments.

A number of characterization techniques are discussed below. More detailed explanations of the physical measurements and use of these techniques are described in Appendix 6.3.

3.1. Electrochemical Aqueous Precursor

Indium nitrated hydrate, gallium nitrate hydrate, and zinc nitrate hydrate in the desired molar fraction were dissolved in 18.2 MΩ H_2O to give a total metal concentration of 0.5 M. In order to drive the formation of a cluster precursor, a platinum working electrode, platinum counter electrode contained in a porous glass frit, and a silver-silver chloride reference electrode were submerged in the solution, as shown in Figure 3. The solution of metal salts was stirred rapidly, and a potentiostat (SP-200, Bio-Logic) was used to apply a potential of -0.49 V at the working electrode with respect to the reference electrode. Aliquots were removed before the constant voltage was applied (so called "salt solutions"), after either 60 and 120 min of electrochemistry or 60 and 75 min of electrochemistry in the case of indium rich solutions. The pH of these aliquots was measured (280GB, IQ Scientific Instrument), and each aliquot was used as a liquid precursor for spin coating.

For dynamic light scattering (DLS) (Mobius, Wyatt Technologies) experiments, the cluster precursor solutions were passed through a 0.45 μm PTFE-45/25 filter and measured at room temperature with 532 nm laser light.
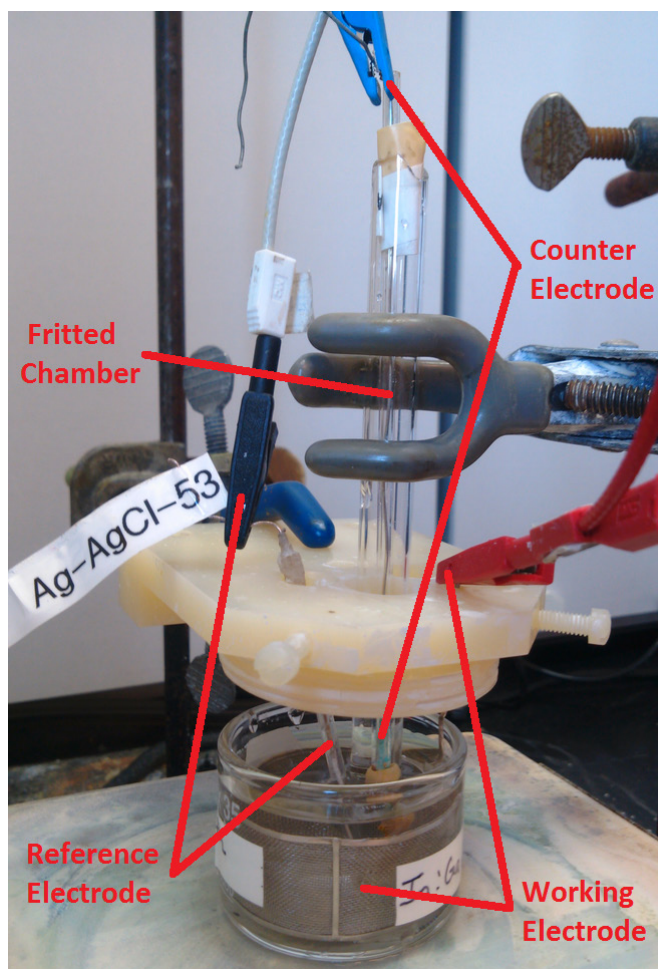
Figure 3. Picture of the electrochemical setup.

A negative potential was applied to the working electrode to reduce chemical species in the main chamber. This resulted in a positive potential at the counter electrode, within the fritted chamber.

3.2. Sol-Gel Precursor

Sol-Gel based precursors were prepared in a manner similar to those reported by Henneck et al.[32] Indium nitrate hydrate, gallium nitrate hydrate, and zinc nitrate hydrate

in the desired molar fraction were dissolved in a 25:1 (v:v) solution of 2-

methoxyethanol and monoethanolamine to give a total metal concentration of 0.5 M.

Solutions were sonicated (1510, Branson) until the metals salts completely dissolved.

3.3. Film Deposition

Silicon (SUMCO Corporation), quartz (Technical Glass Products), p-type doped

silicon, and Au/Ti-coated quartz crystals were used as substrates. Silicon substrates

were cleaned by sonication (3510, Branson) in a 6.25% (v/v) solution of Conrad 70

detergent (Decon Laboratories) and 18.2 MΩ H_2O for 1 h. The remaining substrate

materials were cleaned in a 70°C 3:1 (v:v) solution of conc. aq. H_2SO_4 and H_2O_2 for 10

min, followed by a 15 min oxygen plasma cleaning. Solutions were passed through a

0.45 μm PTFE-45/25 filter prior to spin coating either an aqueous or sol-gel precursor at

1500 RPM for thirty seconds and then at 3000 RPM for forty seconds. The substrates

were immediately annealed on a hotplate at 50°C for 1 min and then at 250°C in either

air or a humid environment for 15 min. Samples requiring additional coats, primarily

for SEM experiments, received the same hotplate annealing regiment between each

coat. Samples used to explore mass loss during annealing, namely samples for QCM

and IR, were instead annealed over a temperature range in a humid environment.

Following spin coating, samples were annealed in either air or forming gas (5% H_2N_2)

at 450°C for 2 h with a 2 h ramp up time.

3.4. Film Characterization

Film morphology were assessed using scanning electron microscopy (SEM)

(Ultra-55, Zeiss) using an accelerating voltage of 5 kV. Film density and thickness were

12

measured using X-ray reflectometry (XRR) (D8 Discover, Bruker) after single layer films were annealed at 450°C for two hours. The effect of annealing on film chemical composition was assessed using quartz crystal microbalance (QCM) (5MHz QCM 200, Stanford Research Systems) and infrared (IR) transmission spectroscopy (6700 FTIR, Nicolet). Films were deposited on Au/Ti-coated quartz crystals for QCM analysis and p-type doped Si for IR analysis. Samples were annealed at 50°C increments from 50 to 300°C for 15 min in a humid environment with measurements being taken at each increment. QCM analysis used changes in frequency to determine the mass loss according to the Sauerbrey equation

$$\Delta f = -C_f \times \Delta m \tag{2}$$

where Δf is the frequency change (Hz), C_f is the sensitivity factor (58.3 Hz μg^{-1}cm^2) of the 5MHz AT-cut quartz crystal,[48] and Δm is the mass change per unit area (μg cm^{-2}).

3.5. Device Fabrication

To fabricate thin film transistor (TFT) devices for exploration of the electrical properties of IGZO, precursor solutions were spin coated on a highly conductive p-type dope Si substrate with a 100 nm surface layer of silicon dioxide. Photolithography and etching in concentrated HCl were used to define isolated rectangles of IGZO. Aluminum contacts were affixed to the top of the IGZO film and arbitrarily designated as drain and source. An additional aluminum contact, designated the gate was affixed to the bottom of the device. Figure 4 shows a schematic of the device.
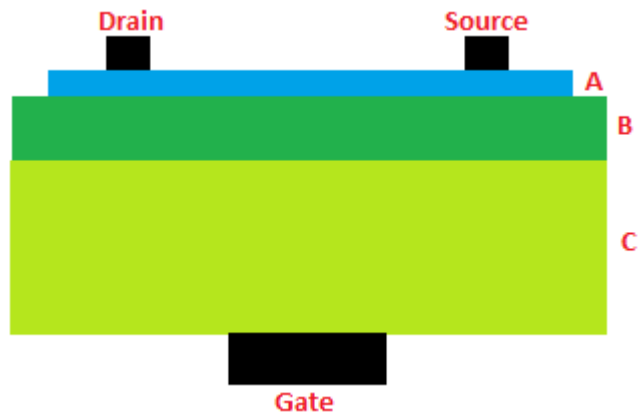
Figure 4. Device schematic.

The drain, source, and gate contacts are made of aluminum and shown in black. Layer A is the IGZO layer (15 nm). Layer B is the insulating gate dielectric (100 nm). Layer C is a highly conductive p-type Si substrate.

4. Results and Discussion

4.1. Solution Chemistry

Unsurprisingly, producing high performance materials via solution based methods relies heavily on the solution, namely the attributes outlined in Section 2: (1) has high solubility (≥ 1 M) in "green" solvents,[41] for instance water and ethanol; (2) contains minimal counter ions and lack of organic ligands that must be driven off; (3) does not readily crystallize upon solvent removal; (4) is stable in solution; and (5) readily cross links after spin coating.[21] In order to engineer a solution precursor with these characteristics, the chemistry of the solution must be understood. Dynamic light scattering (DLS) was the primary technique used to analyze the solution chemistry.

4.1.1. Dynamic Light Scattering (DLS)

To assess the stability of the IGZO precursor, dynamic light scattering (DLS) measurements were performed to measure the size of the IGZO clusters as a function of time and are presented in Figure 5.
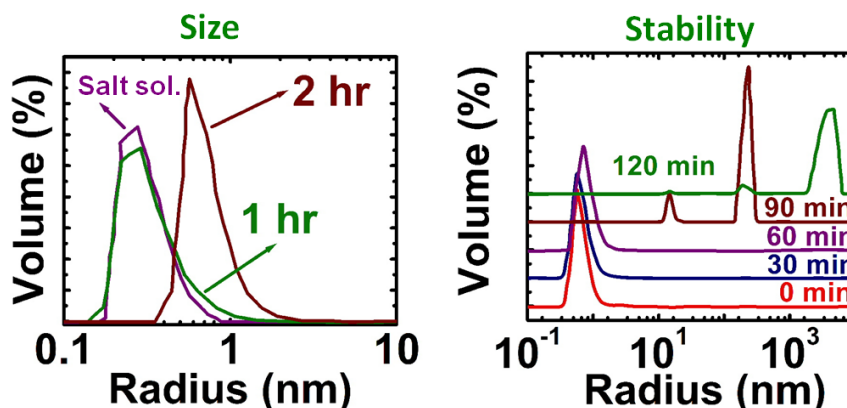
Figure 5. DLS correlation functions.

A solution precursor composition of a 41:33:26 In:Ga:Zn ratio was used. At left, growth of clusters is shown as a function of electrochemistry duration (a). At right, particle size shown as a function of time, demonstrating that the cluster precursor is stable for over an hour at room temperature (b).

Measurements taken as a function of electrochemistry duration, shown in Figure 5a, demonstrate that the formation of clusters with diameters of 1.4 ±0.4 nm. Literature measurements of Ga_{13} clusters report that they do not crystallize into the modified Keggen structure associated with Al_{13} and modified MAl_{12} clusters. Instead, Mensinger et al report that clusters form around a central Ga^{3+} octahedrally coordinated to bridging ligands connecting a ring of six Ga^{3+} which are connected by additional bridging ligands to an outer ring of six additional Ga^{3+}, as shown in Figure 1a.[17] These clusters have diameters of 1.81 nm, but this measurement was taken using single crystal X-ray diffraction of the clusters in the solid state. As a result, this value includes four aquo ligands bonded to each external Ga^{3+} at distances ranging from 0.198 to 0.201 nm that are not necessarily bonded to the clusters formed via electrolysis, suggesting that clusters synthesized here may share the basic structure of the Ga_{13} cluster.

Oliveri et al have analyzed of Ga_{13} clusters in solution by employing H^1 nuclear magnetic resonance (NMR) spectroscopy and diffusion ordered spectroscopies (DOSY)

16

and report a cluster diameter of 2.12 ± 0.08 nm, but these experiments were carried out in DMSO rather than H_2O. Because the Brownian motion measured by both DLS and DOSY is affected by hydrogen bonding to the solvent and the size of the solvent sphere,[49] the size discrepancy may be explained by the difference in solvent. Thus, the Ga_{13} cluster structure reported by Mensinger et al substituted with In and Zn metal ions remains a viable candidate for the structure of clusters formed electrochemically here.

Stability is an important consideration for industrial applications as solutions that precipitate before deposition waste valuable materials. Time dependent DLS measurements, shown in Figure 5b, indicate that the precursor solution is stable for over an hour before the clusters begin to form larger particles with diameters >20 nm. Although solutions prepared using the sol-gel route were stable on the order of days in agreement with literature examples of organic stabilizing agents, such as monoethylamine (MEA),[32,50] diethanolamine (DEA),[24] and acetylacetone,[51] the one hour stability window of the cluster precursor is still sufficient to produce films of over 100 nm with an annealing step in between each coat.

4.1.2. Intermediaries

In conducting this experiment, a qualitative picture of the solution chemistry was assumed. The negative potential at the working electrode drives reduction. To maintain charge balance, the positive potential oxidizes water, resulting in observable oxygen evolution. Currently, it is unclear whether H^+ (to form H_2) or NO_3 (to form NO_x or ammonium) is being reduced. While the formation of neither gaseous product was observed, the working electrode has sufficient surface area that these products may form bubbles too small to see. Reduction of either or both of these species increases the

pH of the main chamber, driving cluster formation as the solution pH moves toward the phase boundaries shown in the Pourbaix diagrams, presented in Figure 6 for group 13 metals and in Figure 9 for zinc. However, cluster formation does not take place immediately–the 1 h electrolysis DLS curve, shown in Figure 5a, closely resembles the shape of the salt solution curve, indicating that the particles in each solution are of similar size.
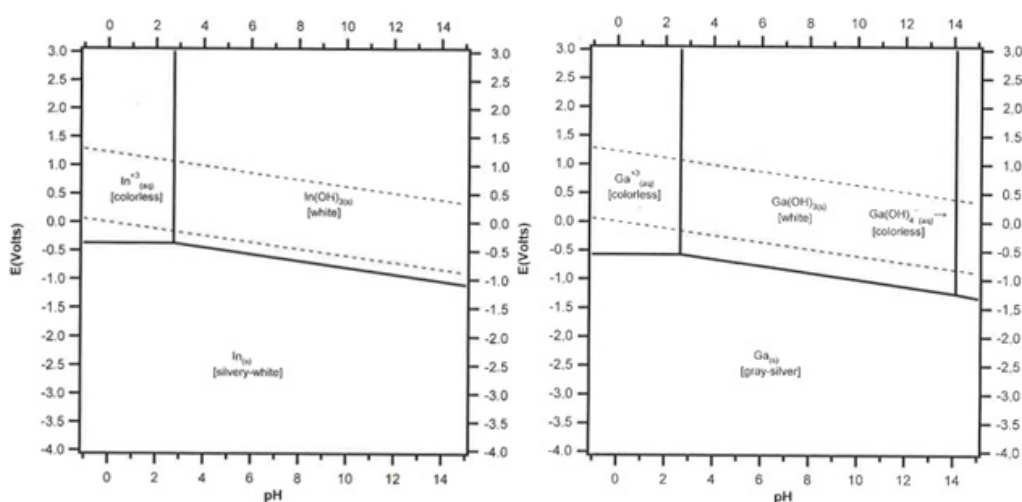
Figure 6. Pourbaix diagrams for indium (left) and gallium (right).[20]

The area of interest lies between the dotted lines, with the solution pH beginning in the range of the aqueous species and approaching the phase boundary.

Despite a lack of observed change in particle size after one hour of electrolysis, chemical reactions are occurring in the solution. The pH of the solution, shown as a function of electrolysis duration in Figure 7, increases linearly as electrolysis occurs across a diversity of solution compositions, indicating that oxidation is occurring at the working electrode as described above.
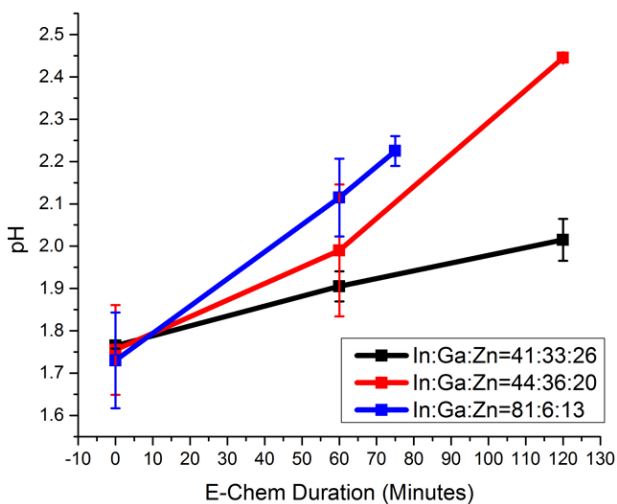
Figure 7. Solution pH data.

The pH at the working electrode as a function of electrolysis duration is shown for a representative sample of IGZO compositions. More rapid change in pH is likely attributable to a lower presence of zinc whose phase boundary is at a pH of 6.5 rather than at a pH of 2.5, like that of indium and gallium.

The pH changes in solution are likely evidence of intermediaries between individual metal aquo complexes and clusters; it is highly unlikely that the ligands of 13 ions simultaneously connect to form clusters in a single step. A schematic of likely early intermediaries is shown in Figure 8. Initially, aquo ligands stabilize the metal ion in solution, forming the initial octahedral species. The metal ion draws electron density form the surrounding oxygen, resulting in positive charge build up on the hydrogen atoms. As a result, the bond between the hydrogen and oxygen is weakened, allowing water molecules to deprotonate the water ligands. This is why the salt solutions have low pH values. In accordance with Le Chatelier's principle, the loss of hydrogen ions resulting from the electrochemically driven pH change increases the frequency at which deprotination of the metal aquo complex occurs. As the pH of the solution further increases and the deprotinated species begin to bump into each other, the hydroxyl

19

ligand can form a bridge between metal ions, generating the final species shown in Figure 8. These intermediaries may substitute their aquo ligands for additional hydroxyl bridging ligands, eventually creating the cluster core of six metal ions connected via hydroxyl bridging ligands to a central, octahedral coordinated metal ion. Similar ligand substitution on the six exterior metal ions may generate the final 13 metal ion cluster.
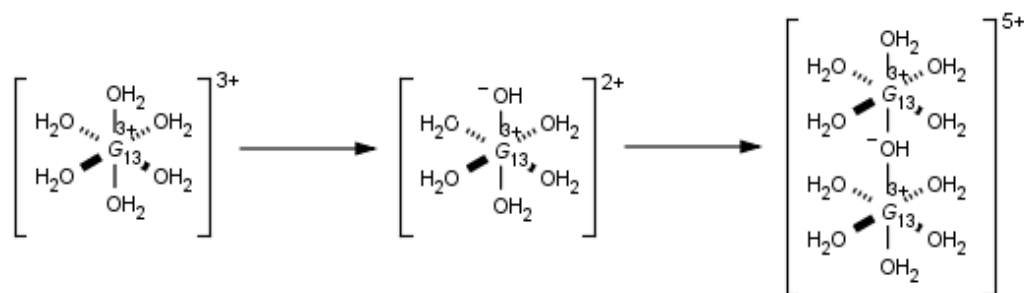
Figure 8. Proposed intermediaries for cluster formation.

Initially, the metal ion, shown with a group 13 placeholder, is stabilized by an octahedrahal arrangement of water ligands. As the pH of the solution increases, deprotonation of the water ligands occurs with greater frequency. When the hydroxide ligand comes in contact with another metal ion, it can displace a water ligand to form a hydroxyl bridge between the two ions.

While the intermediaries described above are consistent with the DLS and solution pH data, there are limitations to this speculative analysis. There exist numerous other possibilities for the cluster formation mechanism. For instance, the metal ions might initially form a peroxide bridge that reacts with the hydronium in solution to form the hydroxyl bridge. In addition, the addition of high numbers of metal ions may occur differently. For instance, multiple metal ions might become joined by hydroxyl bridges and then fold into clusters rather than adding to a single metal ion. Finally, because zinc ions have different oxidation states than indium or gallium ions (Zn^{2+} rather than In^{3+} or

Ga^{3+}), indium gallium zinc clusters might have entirely different, but similarly sized, structures than the Ga_{13} clusters[17] and Ga_7In_6 clusters[19] reported in the literature.

Interestingly, despite not forming appreciable numbers of clusters, the 1 h solutions still made high performance films. This indicates that the intermediary species might crystalize sufficiently slowly to prevent rapid crystallization into isolated grains upon solvent removal. This has implications for zinc substitution into the mixed metal cluster, particularly given that zinc has a different oxidation state than the group 13 metals and that zinc is water soluble over a much greater pH range than the group 13 metals, as evidenced by the zinc Pourbaix diagram in Figure 9.[20] However, the 2 h electrolysis DLS curve indicates that there are no species with diameters of <0.6 nm in solution, meaning that the aquo zinc species are consumed in the cluster formation reaction.
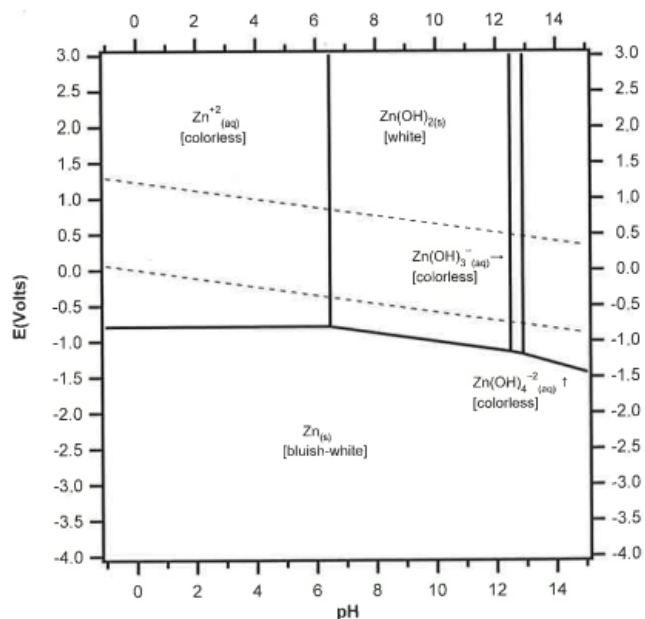
Figure 9. Pourbaix diagram for zinc.[20]

The area of interest lies between the dotted lines, with the solution pH beginning in the range of the aqueous species and approaching the phase boundary.

4.2. Morphology

Figure 10 shows SEM images of a representative sampling of IGZO compositions. Both salt solution films (Figure 10a,c,e) and cluster films (Figure 10b,d,f) are shown for a variety of metal compositions. In addition, films synthesized via the Sol-Gel route are shown in Figure 11.
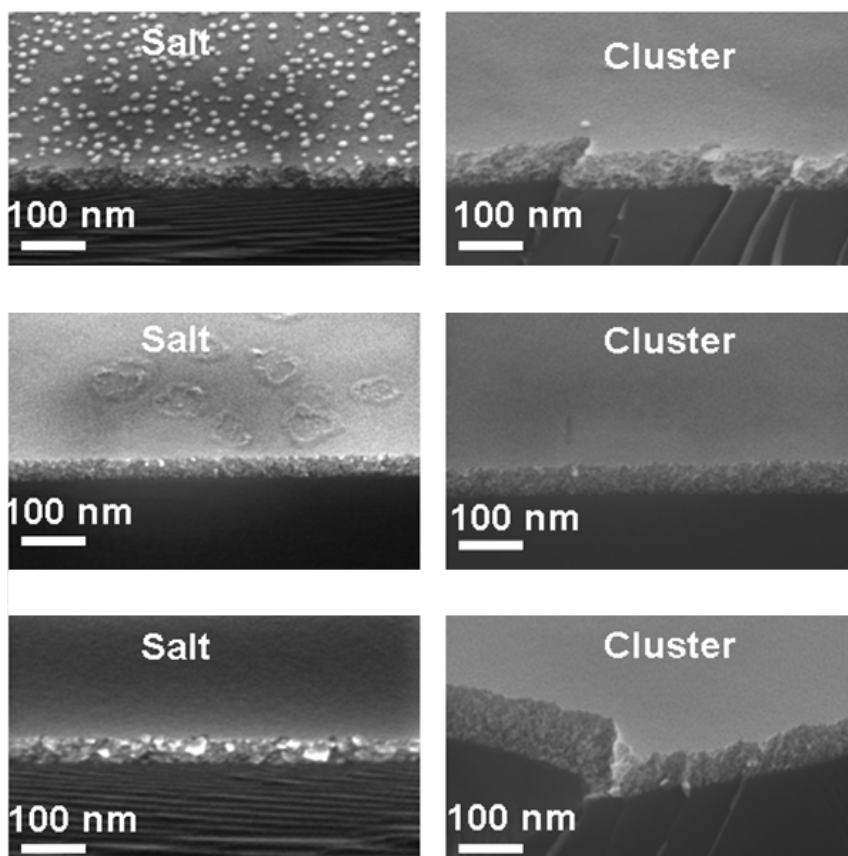
Figure 10. SEM images of IGZO films produced using electrochemical precursor.

Images taken at a 45° tilt of films prepared by spin coating three layers of a salt solution (left column) and a cluster precursor (right column) are shown for a representative sampling of IGZO compositions: (a-b) 32:26:42 In:Ga:Zn ratio; (c-d) 41:33:26 In:Ga:Zn ratio; and (e-f) 81:6:13 In:Ga:Zn ratio.
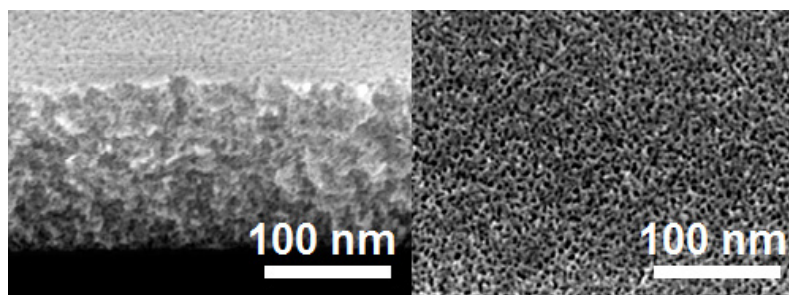
Figure 11. SEM images of IGZO films produced using the sol-gel method.

A 45° tilt view is shown on the left, and a top-down view is shown on the right to emphasize the film roughness. The sample has a 41:33:26 In:Ga:Zn ratio.

The surfaces of the salt solution films, particularly those shown in Figure 10a and Figure 10c, are rough, with features visible on the surface of the film. Absent electrochemistry, salt solutions readily crystallize when the solvent is removed during spin coating, forming individual crystals rather than a uniform film. These features are especially prominent in Figure 10a. Initially, these features appear to only be on the surface of the film, but an examination of the film cross section reveals grains of nearly the same size. While the formation of extraneous features on the surface of the film has a relatively minor impact on the film performance, the appearance of these features throughout the film is problematic because they generate grain boundaries that are not bridged by molecular orbitals (see Appendix 6.1.2). This necessitates electrons tunnel through the boundary to move freely across the material, decreasing carrier mobility, an important characteristic for electrical applications. The large grain size of the films produced using salt films is especially apparent in Figure 10e which contains grains as large as 25 nm in diameter.

In contrast, the films produced using cluster precursors show markedly smaller grains. Figure 10b shows a single example of the features populating the surface of the film in Figure 10a which is much larger than the individual grains in the film that are difficult to pick out. Figure 11 presents a film produced using the sol-gel method. While this film does not have any features protruding from the surface of the film, top-down SEM images reveal that the surface of the film is quite porous. The porosity results from the removal of the organic solvent and stabilizing agent (here 2-methoxyethanol and monoethanolamine, respectively) in addition to the counter ions that must be removed from all films.

24

SEM images do expose an advantage of the sol-gel method: it yields a thicker film than the cluster precursor solutions do. In turn, the cluster precursor yielded thicker films than the salt solution at every metal composition. However, this disadvantage can be compensated for by simply depositing more layers via spin coating, and DLS analysis indicates that cluster precursor solutions are stable for long enough to allow several depositions.

4.3. X-Ray Reflectivity (XRR) Analysis

XRR patterns were fit using REFS (Bede Scientific Inc.) yielding film density and thickness for the sol-gel, salt solution and cluster precursor films after films were annealed for 2 h at 450°C (Figure 12). The XRR data confirms observations made using SEM images, namely that the sol-gel method produces the least dense but thickest films.
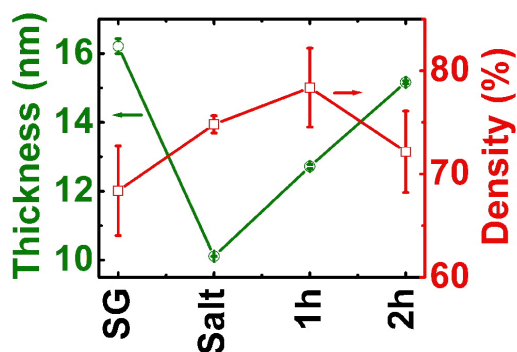
Figure 12. Results of XRR analysis.

Film thickness and density shown for films made using a sol-gel precursor, salt solution, 1 h electrochemical precursor, and 2 h electrochemical precursor for a 41:33:26 In:Ga:Zn ratio.

Multiplying the thickness by the density for the sol-gel and both electrolysis samples yields the same value with experimental uncertainty which is expected given

that all precursor solutions share the same metal concentration. This underscores the problems associated with simply using the salt solution as a precursor as its metal usage is not nearly as efficient.

The most unexpected feature of the XRR data is the decline in density between the films produced using the 1 h and 2 h electrochemical precursors. Assuming that the analysis made of the intermediaries in Section 4.1.2 is correct, this drop might be explained by the structural constraints imposed by clusters. Rather et al report that for the Ga_{13} cluster, the bond lengths of the metal oxygen bond are 0.196 to 0.215 nm for the ligands bridging the inner gallium ring to the core gallium, 0.191 to 0.192 nm for the ligands bridging the inner and outer gallium rings, and 0.198 to 0.201 nm for the external water ligands.[17] Particularly given the existence of exterior water ligands which form hydrogen bonds with the exterior water ligands of other clusters, this is not the most efficient way to pack metal ions. Alternatively, after the 1 h electrochemistry solution is deposited, it likely begins to cross link immediately, forming oxygen bridges between metal ions as water leaves the film. As a result, the metal ions might be packed more tightly, resulting in a more dense film.

Interestingly, the electrochemistry produces films up to 150% thicker than the salt solution despite both the salt and cluster solutions having total metal concentrations of 0.5 M. Because XRR was only performed after samples were annealed at 450°C, this data is insufficient to explain the differences in thickness among the cluster films. Instead, the thickness difference is discussed in Section 4.4.2.

4.4. Annealing

Once solutions are deposited via spin coating or other techniques, atoms are not necessarily in the most favorable positions from an energetic standpoint. Annealing gives sufficient energy to overcome the activation barrier for rearrangement to more thermodynamically favorable configurations. Put another way, heating atoms causes them to vibrate, and sufficiently large vibration creates enough space between atoms for them to rearrange into positions that require less energy. Crystal lattice structures are generally energetically favorable, and amorphous IGZO will begin to crystallize at temperatures >550°C.[8] For TCOs, this is fairly high temperature, affording a large thermal range for annealing to accomplish its other purpose: driving off unwanted species.

Unlike in organic synthesis, it is often difficult or impossible to remove impurities following inorganic synthesis. However, some impurities can be removed via annealing. Heating can speed the rate of evaporation and condensation reactions, removing excess water from solution. Some unwanted impurities, such as some organics and nitrates, decompose into gaseous products at high temperatures, leaving the film. However, because the film is in the solid phase, it cannot fill in the vacancies left by these species, leaving pores in the film.

4.4.1. Low Temperature to Humid Annealing

As described in Section 3.3, samples used for device fabrication were annealed in multiple steps. Samples were annealed on a hotplate in air at 50°C for 1 min and subsequently were annealed on a hotplate in a humid environment at 300°C for 15 min. The initial 50°C annealing step was designed to trigger condensation reactions in the

film to remove excess water. Annealing at a higher initial temperature runs the risk of triggering all condensation reactions simultaneously and vaporizing the water. The associated volume change has the potential to damage the film. Following this annealing, the sample was transferred to a 300°C hotplate with a wet atmosphere. Wet annealing prevents desorption of oxygen species which is problematic because oxygen deficiencies cause electron trapping that undermines electrical performance.[52] Watanabe et al have explored this phenomenon. Oxygen desorption occurs when O_2 reaches an active site capable of splitting the molecule. The product of this splitting can react with oxygen in IGZO to reform O_2. Oxygen diffusion experiments show that water vapor reacts with the IGZO surface preferentially to O_2, resulting in the formation of terminal hydroxides on the surface of the film. This surface feature shields active sites from splitting oxygen.[53]

4.4.2. Quartz Crystal Microbalance (QCM) Analysis

Mass loss as a function of annealing temperature (50-300°C) was precisely measured using QCM analysis, shown in Figure 13. Both films showed no change between annealing at 250°C and annealing at 300°C, and the cluster precursor film had nearly reached its final mass after being annealed at 200°C. This indicates that the cluster precursors lower the prerequisite annealing temperatures for solution processed IGZO.
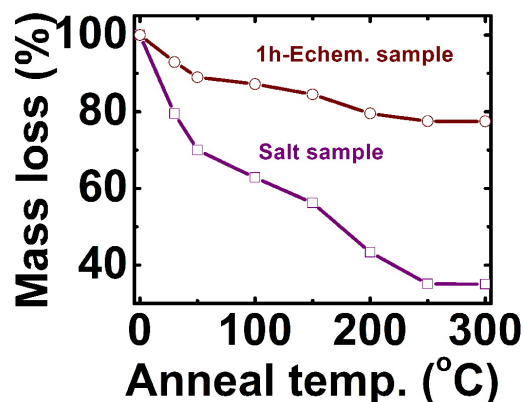
Figure 13. Results of QCM analysis.

Mass loss, shown as a percent of original mass, plotted as a function of annealing temperature. Films made using a salt solution and a 1 h electrochemistry solution, both with a 70:15:15 In:Ga:Zn ratio, are shown.

Interestingly, the QCM results indicate that the salt precursor films lose substantially more mass than the cluster precursor films upon annealing; the salt precursor film loses 63% of total mass compared to the cluster precursor's 21%. This difference is attributable to the chemical processes that take place during electrolysis. As reduction and oxidation take place at the working and counter electrodes, different species are consumed on either side of the frit. In accordance with Le Chatelier's Principle, species diffuse across the frit in order to maintain equilibrium. In this particular instance, metal ions move from the counter electrode to the working electrode and nitrates move from the working electrode to the counter electrode. As a result, aliquots taken from near the working electrode have a higher concentration of metal ions relative to nitrates, leaving fewer counter ions to be removed following deposition. The result of this substantial mass loss can be seen in the XRR analysis; 2 h electrolysis films are 150% as thick as salt solution films, despite both precursor solutions ostensibly having the same metal ion concentration.

4.4.3. Infrared (IR) Transmission Spectroscopy

IR spectroscopy was used to characterize the chemical composition of the mass loss. The IR spectrums, shown in Figure 14, contain peaks characteristic of nitrate (1200-1600 cm^{-1}) and hydroxyl (3000-3800 cm^{-1}) groups. Consistent with the QCM data, both peaks vanish after the film is annealed at 200°C.
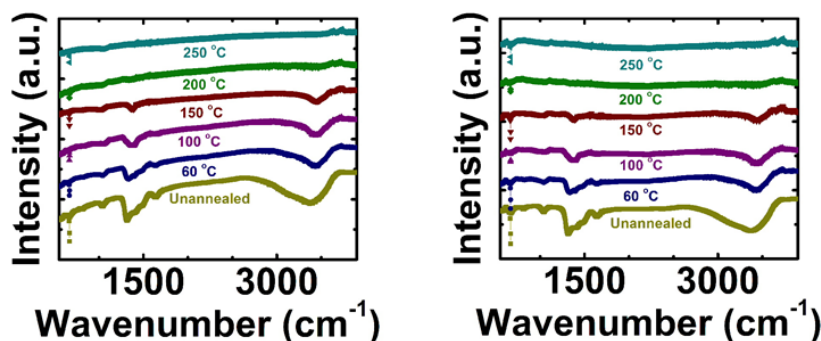
Figure 14. IR spectrums of films made using a salt solution (left) and a 1 h electrochemistry precursor (right).

Both films have a 70:15:15 In:Ga:Zn ratio. The peaks correspond to nitrate (1200-1600 cm^{-1}) and hydroxyl (3000-3800 cm^{-1}) functional groups.

IR data confirms the rational for the initial annealing step at 50°C. Annealing at low temperatures drives off both nitrate and hydroxyl containing species, evidenced by the difference in size of the peaks characteristic of these functional groups in the unannealed and 60°C curves.

Both the QCM and IR data indicate that complete mass loss occurs after annealing at 250°C with nearly all mass loss occurring at 200°C. These results are promising for making solution processing compatible with the plastic substrates necessary for flexible electronics. The lower requisite annealing temperature in comparison to sol-gel films is attributable to fewer materials requiring removal following deposition. For cluster based films, IR analysis shows only nitrate and

hydroxyl containing compounds leaving the films—no organics are involved in the synthesis.

4.5. Device Properties

Given that transistors are the principle application of IGZO, the performance of devices fabricated using IGZO are an important litmus test of the synthetic method. Dr. Nadarjah performed measurements on thin film transistors (TFTs) fabricated using IGZO of a variety of compositions at Oregon State University. A discussion of the properties being measured may be found in Appendix 6.1.3 while a description of the measurements being taken may be found in Appendix 6.3.6. Figure 15 shows an average channel mobility plot of films produced using salt solution and two electrolysis precursors. Although all films shown in Figure 15 have an In:Ga:Zn ratio of 69:12:19, the greater average channel mobility of the cluster precursor films is seen across all compositions, vindicating other measurements suggesting that the electrochemistry improves film quality.
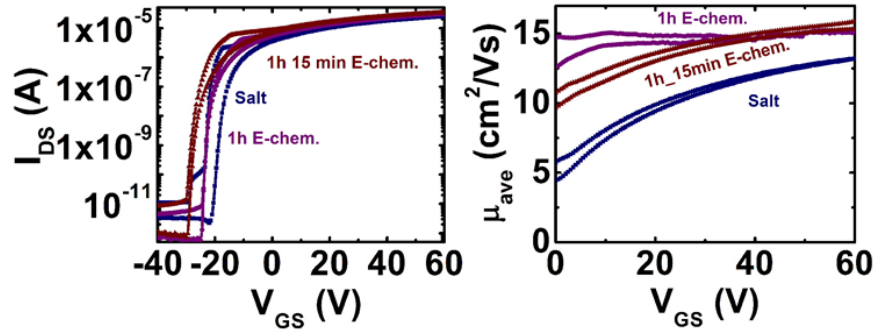
Figure 15. Comparison of electrical performance across electrolysis duration.

Transfer curve and average channel mobility plot showing motilities of films produced using salt solution, 1 h electrolysis, 1 h 15 min electrolysis precursors for an In:Ga:Zn ratio of 69:12:19.

Given that electrochemical precursors produce higher performance films than salt solution precursors, the composition of the IGZO layer is the next variable to explore to improve film quality. Figure 16 shows transfer curves and average channel mobility plots for a variety of IGZO compositions, and Table 1 summarizes the average channel mobility and turn-on voltage for each composition.
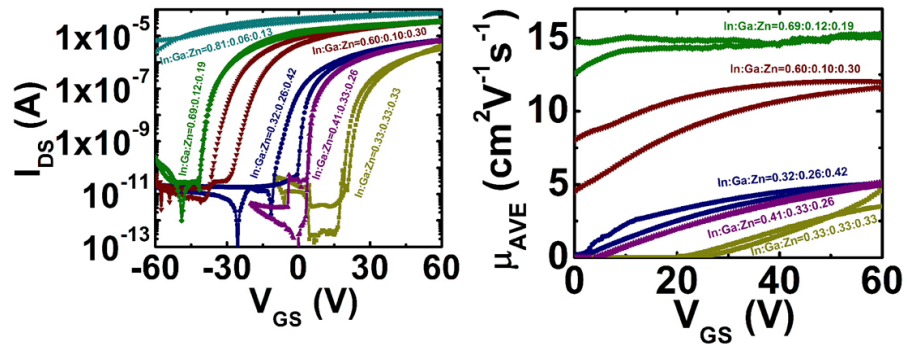
Figure 16. Transfer curve and average channel mobility plot for a range of IGZO compositions.

An In:Ga:Zn ratio of 69:12:19 can be seen to yield the highest average channel mobility. The results of these plots are summarized in Table 1.

Films produced with an In:Ga:Zn ratio of 69:12:19 performed best with an average channel mobility of 15.2 cm^{2}V^{-1}s^{-1}. In addition, this composition displayed an

32

on/off current ratio of $>10^6$. The high performance of the indium rich film may be attributed to the physical explanation for conductivity in amorphous materials (see Appendix 6.1.2). Electrons travel via the large s-orbitals associated with the metal atoms.[54] While for gallium and zinc this is the 4s orbital, indium's valence electrons occupy the 5s orbital, which is larger and thus results in fewer interruptions of the electron's path through the material.

Composition (In:Ga:Zn)	μ_{avg} (cm^{2}V^{-1}s^{-1})	~V_{on} (V)
33:33:33	4.1	20
41:33:26	4.9	2
32:26:42	5.1	-2
60:10:30	11.5	-33
69:12:19	15.2	-40
81:6:13	—	—

Table 1. Summary of average channel mobility and turn-on voltage for devices fabricated with a variety of IGZO compositions

Comparing the mobility of this film with literature values is difficult, owing to the fact that a number of other mobilities are traditionally reported in place of the average channel mobility such as the effective mobility, the field effect mobility, the saturation mobility, and the Hall mobility. However, the field effect mobility is defined similarly to the average channel mobility with the threshold voltage replacing the turn-on voltage.[55] Both sol-gel and vacuum deposition films have field effect mobilities in the range of 1-20 cm^{2}V^{-1}s^{-1} with ~10 cm^{2}V^{-1}s^{-1} generally being the expected value for an IGZO device.[30,32,35,51] Thus, IGZO produced using electrochemical precursors yields high performance films without using techniques that employ high processing temperatures, costly and unsafe organics, or high vacuum conditions to deposit films.

4.6. Cluster Synthesis in the Literature

4.6.1. Literature Cluster Synthesis Comparison

Significant room for study of the chemistry underpinning the precursor solutions synthesized here exists because no research has come close to considering an electrochemical cluster route for IGZO. While efforts have been made to synthesize IGO[19] and amorphous aluminum indium oxide (AIO)[56] using cluster precursors, these studies pursued different materials and did not employ electrolysis to produce clusters, instead relying on crystallization reactions necessitating several days for solvent evaporation. Studies that have employed electrochemistry to synthesize nanoclusters have focused different materials, such as aluminum oxide,[22] and emphasize solution characterization with tools such as Raman spectroscopy over film formation. The closest analog to our procedure, perhaps unsurprisingly, comes from our own group and explores electrochemical synthesis of F-modified tin (II) hydroxide nitrate nanoscale clusters for the synthesis of F-doped tin (IV) oxide.[21] However, the challenge associated with developing an SnO_2 aqueous precursor stems from insolubility of Sn^{4+} except in extremely acidic conditions (<pH 0). In contrast, nitrate salts of In^{3+}, Ga^{3+}, and Zn^{2+} are all soluble in water, as the nitrate ions acidify the solution (pH 1-2).[20]

Instead, generating appropriately sized and stable clusters is the greatest challenge associated with IGZO cluster synthesis. If insufficient cluster formation occurs, rapid crystallization upon spin coating generates the rough films seen in the SEM images of the salt solution films shown in Figure 10. On the other hand, if electrochemistry is run for too long, the potential is driven across the phase boundary, resulting in the solution precipitating and becoming unusable. DLS data, shown in

Figure 5 exposes a happy medium between these extremes. The growth of clusters with 1.2 nm diameters can be seen beginning after 1 h electrolysis, with this peak fully growing in after 2 h of electrolysis. While longer electrolysis will cause the clusters to crash out of solution, the solution is stable at room temperature for up to ninety minutes, which is confirmed by the DLS stability data.

Interestingly, as the indium content is increased, the solution begins to precipitate after a shorter duration of electrochemistry. As a result, indium rich (70:15:15 In:Ga:Zn ratio) cluster precursors were synthesized with 1 h or 75 min of electrolysis, compared to the 1 h or 2 h electrolysis used for other In:Ga:Zn ratios. This is in line with the literature which has isolated few indium clusters.[14]

4.6.2. *Literature IGZO Solution Processing Comparison*

Although similar electron mobilities in IGZO films have been reported elsewhere,[30,32,35,51] the films produced here are unique in that they reduce the requisite processing temperatures from 300°C for conventional sol-gel films to 200-250°C. This drop is particularly important because it crosses the threshold necessary to enable solution processing routes to be employed in flexible electronic applications on plastic substrates.[36]

Attempts have been made to apply sol-gel methods to plastic substrates. The 'sol-gel on chip' method uses conventional sol-gel processing and deposition followed by addition of an aqueous catalyst to the film to replace organic ligands at processing temperatures in the range of 200-300°C. Although it was not the principal focus of their study, Banger et al synthesized indium rich IGZO films that achieved maximum effective mobilities of 4.05 $cm^2V^{-1}s^{-1}$ annealing at 275°C and of 6.12 $cm^2V^{-1}s^{-1}$

annealing at 350°C.[25] Here, an average channel mobility of 15.6 $cm^2V^{-1}s^{-1}$ was achieved with a similar composition (In:Ga:Zn ratio of 69:12:19 versus 63:10:27). The improvement in mobility is likely due to the lack of organic ligands that must be removed the aqueous precursor solution.

In addition to using alternative deposition techniques to reduce the processing temperature of sol-gel films, researchers have explored alternative annealing techniques. Namely, excimer laser annealing (ELA) can be used to selectively increase the temperature of IGZO to 1500°C without damaging substrates sensitive to heat in excess of 150°C. However, this requires substantially thickening the gate dielectric. For a 100 nm thick SiO_2, the same thickness used in this study, the substrate reached temperatures in excess of 600°C; increasing the thickness of this layer to 600 nm is necessary to prevent the substrate temperature from rising above 150°C.[57] In addition, while this technique does lower the maximum temperature of the substrate, it still has the disadvantage of employing an organic stabilizing agent that leaves the film porous on removal. This is readily seen in the SEM images reported by Tsay and Huang. Their highest performing film, produced by conducting ELA with a laser density of 350 $mJcm^{-2}$, is reproduced in Figure 17, and displays significant porosity in contrast to the SEM images presented here in Figure 10.
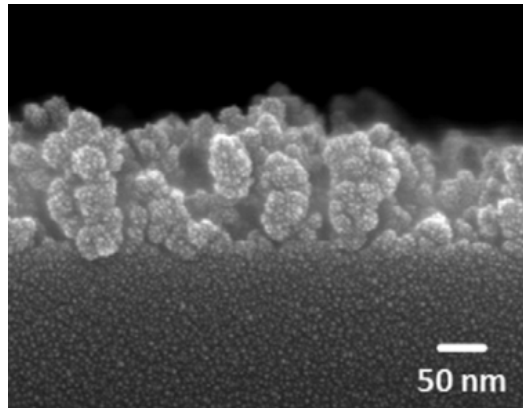
Figure 17. SEM image of IGZO produced via ELA.[36]

The sample was annealed using a laser energy density of 350 mJcm^{-2}. The film has an In:Ga:Zn ratio of 1:1:2, and exhibits a Hall effect mobility of 5.26 cm^{2}V^{-1}s^{-1}.

5. Conclusion

A previously unreported nanoscale cluster composed of indium, gallium, and zinc was synthesized using a method that has only been applied to a handful of materials. Exploration of both the cluster structure and mechanism provide promising avenues for future research and is necessary to determine if this method produces harmful NO_x byproducts. In addition, the electrochemical method has potential to be applied to the development of aqueous precursors for other materials.

The IGZO films fabricated into devices outperformed not only salt solution films but also many sol-gel, PLD, and magnetron sputtering films. IGZO composed of a 69:12:19 In:Ga:Zn ratio displayed an average channel mobility of 15.2 $cm^2V^{-1}s^{-1}$, turn-on voltage of ~-40 V, and an on/off current ratio $>10^6$. Importantly, this film was synthesized from a concentrated (0.5 M) all inorganic aqueous precursor solution that QCM results suggest contains fewer counter ions than even the salt solution. Because of this, these films require lower annealing temperatures of 200 to 250°C, allowing solution methods to be applied to flexible electronics. In addition, DLS shows that these precursor solutions are stable for up to 90 min, a sufficient length of time to allow multiple depositions from the same solution. Finally, these precursors seem to occupy the happy medium between crystalizing too quickly upon solvent removal to yield rough films and failing to cross link at low annealing temperatures; SEM images show that the electrochemistry precursor films are smooth while XRR analysis shows that they are dense.

6. Appendix

6.1. Band Theory and Electrical Properties

Band theory describes electrons in chemical structures with long range order or, in other words, structures that contain lattice points such that a unit cell bounded by these points can be translated to form the structure. Many of the useful properties of semiconductors and specifically transparent conducting oxides (TCOs) can be explained by band theory.

6.1.1. Band Theory

Band theory arises from quantum mechanics. The individual behavior of an electron is described by the wave function, Ψ, according to the Schrodinger equation, stated time-independently as

$$E\Psi = \hat{H}\Psi \qquad (3)$$

However, as a consequence of the Pauli Exclusion Principle, no two electrons may be indistinguishable, substantially complicating the picture of electron behavior in systems with molar quantities of electrons. To deal with this, it is necessary to step back and consider groups of electrons.

Often, it is easier to think of electrons in terms of atomic orbitals which are constructed by taking linear combinations of allowable wave functions. When chemical bonding occurs, it may be described mathematically in terms of interactions between the valence orbitals of each atom. Taking a linear combination of atomic orbitals gives rise to molecular bonding orbitals, which have an energy minimum when the nucleuses of each atom are of a particular distance from each other, and molecular antibonding

orbitals, which increase in energy as the nucleuses of each atom come together. Because lower energy configurations are favorable, occupied bonding orbitals incentivize atoms to reside at a particular distance from each other and form a chemical bond while antibonding orbitals incentivize atoms to move away from each other. When a large number of atoms are present, orbitals can be arranged in either a bonding or an antibonding state. Once again, a linear combination of wave functions, so called Bloch functions, is used to describe the system of n atoms

$$\psi_k = \sum_n e^{ikna} \chi_n \tag{4}$$

where k is an index, a is the distance between lattice points, and χ is a basis function describing a particular orbital. Embedded within k is information describing whether orbitals are arranged in a bonding or antibonding fashion. In order to avoid counting configurations repeatedly, k is bounded on the range $|k| \leq \pi/a$, referred to as the first Brillouin zone. The Brillouin zone contains n values of k which can be plotted in the space of k, a space in which each value of k is equally spaced, as shown in Figure 18 for a one dimensional chain of hydrogen atoms.
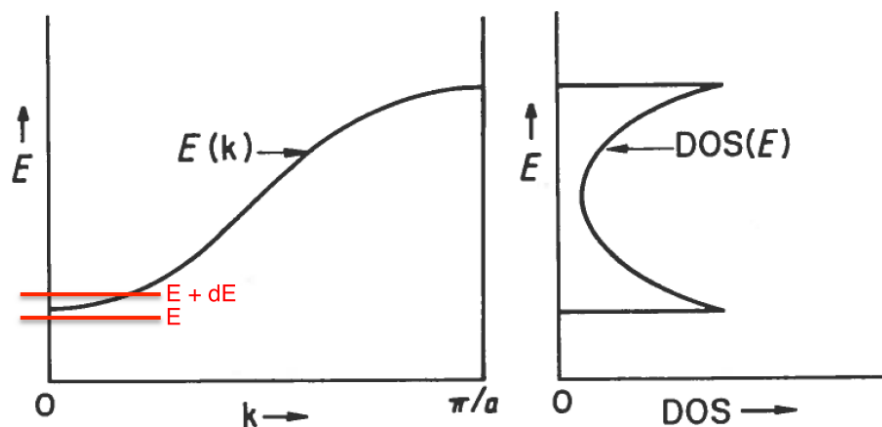
Figure 18. Band structure (left) and density of states plot (right) for the 1s orbitals of a one dimensional string of hydrogen atoms.[58]

Because such plots can be cumbersome when considering multiple orbitals, such as in Figure 19, it is useful to think about the frequency of energy levels rather than individual energy levels. This is accomplished with a density of states plot, defined as

$$DOS(E) = \text{number of levels between } E \text{ and } E + dE \qquad (5)$$

Integrating the density of states plot gives the number of molecular orbitals within the range of integration. As a result, the energy of the highest occupied molecular orbital (HOMO), E_{HOMO} can be expressed for the lowest possible energy configuration of the system can be expressed as

$$n = \int_0^{E_{HOMO}} DOS(E)dE \qquad (6)$$

for a system containing n electrons. While a slight simplification, the energy of the HOMO may be thought of as the Fermi level. In Figure 19, the Fermi level lies at the top of the z^2 band in the band structure plot and at the same energy level in the DOS plot.
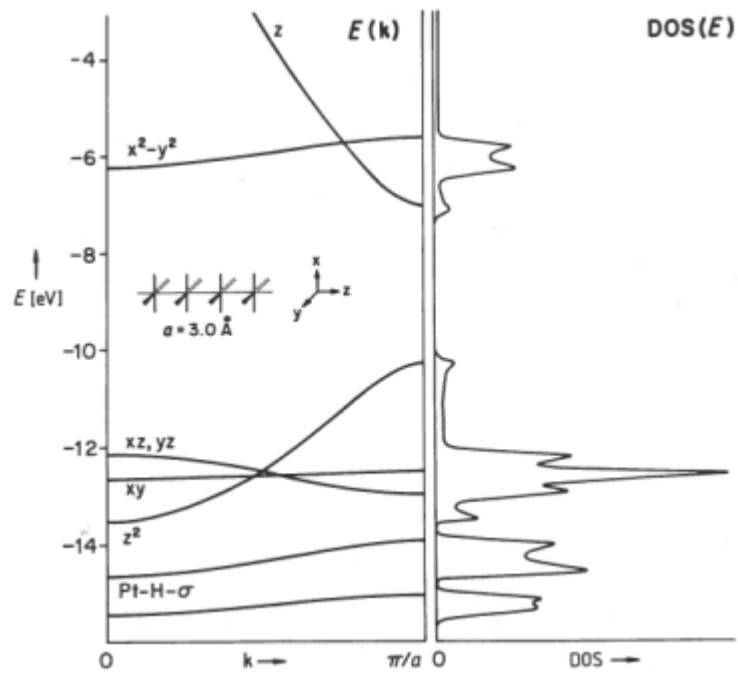
Figure 19. Band structure and DOS plots for PtH_4^{2-} atoms.[58]

The atoms are arranged along a line such that two planes bisect are sufficient to bisect all of the hydrogen atoms.

The location of the Fermi level relative to the density of states has important consequences for the properties of a material. When an electron is excited above the Fermi level, it can move around the crystalline structure. As a result, materials with unoccupied states that are close in energy to the Fermi level more easily conduct electricity. The distance between the Fermi level and the next unoccupied state is referred to as the band gap. Collectively, the states below the Fermi level are known as the valence band while the states above the Fermi level are called the valence band. Because the band gap has such a substantial impact on the properties of a material, it is used to classify them: materials whose Fermi level bisects a band are known as metals; those with band gaps are small enough that thermal energy can promote electrons to

unoccupied orbitals are referred to as semiconductors; and those with large band gaps are known as insulators.[58]

6.1.2. Conductivity, Carrier Concentration, and Mobility

Because conductivity is such an important property of semiconductors, further discussion is warranted. Electrical conductance is defined as the reciprocal of the electrical resistance and is reported in siemens (S). In order to quantify these properties for a given material, the conductance and the resistance must be normalized by the thickness of the material. These normalized quantities are referred to as the conductivity and resistivity, respectively. Although the SI unit of conductivity is siemens per meter (Sm^{-1}), convention dictates that conductivity be reported in units of siemens per centimeter (Scm^{-1}). The electrical conductivity, σ, may be expressed as a function of the carrier concentration, N; the carrier charge, e; and the mobility, μ, as

$$\sigma = Ne\mu \tag{7}$$

Here, the carrier concentration is given in carriers per cm^{-3}, the carrier charge in coulombs (C), and the mobility in $cm^2V^{-1}S^{-1}$. Because carrier charge is a physical property of the charge carrier, it is constant. Thus, the conductivity varies with the carrier concentration and mobility.[59] The carrier concentration is a consequence of band theory; it is the number of charge carriers (electrons or holes) in the conducting band present in a material per unit volume.

Mobility refers to the ease with which a charge carrier may move through a given material. It may be expressed in terms of the average scattering time, τ, and the carrier effective mass, m^*, as

$$\mu = \frac{e\tau}{m^*} \tag{8}$$

where μ and e are as defined in Equation (**7**. Equation (**8** indicates that either increasing

the average scattering time or decreasing the effective mass will increase the mobility.

Decreasing the effective mass involves new material development while increasing the

scattering time pertains to improving film quality. In the case of crystalline TCOs,

improving the film quality requires controlling the ordering of atoms in the material on

a nanoscale because a well ordered material gives electrons or other charge carriers a

uniform path to move across without being impeded by grain boundaries.

Unfortunately, this generally necessitates high temperature processing, which is

wasteful and can impede application. Alternatively, amorphous materials can also

exhibit high motilities (10-50 $cm^2V^{-1}S^{-1}$). Although irregularities in the periodic electric

potential generally inhibit the mobility of amorphous structures, it has been

hypothesized that metals with electron configurations of the form $(n-1)d^{10}ns^0$, for $n > 4$,

achieve conduction via overlapping s-orbitals, allowing for unimpeded carrier paths

despite a lack of long range ordering.[54]

6.1.3. *Thin Film Transistor (TFT) Properties*

Transistors are semiconductor devices that act as on/off switches that react to a

potential. Three important properties of transistors are the turn-on voltage, V_{on}, the

average channel mobility, μ_{avg}, and the on/off current ratio. The turn-on voltage refers

to the voltage at which the transistor switches from off to on. Values that are closer to

zero in either the negative or the positive direction are preferable because devices with

these values require less energy to operate. One way of representing the mobility of a

transistor is as the slope of the transfer curve or average channel mobility. More precisely the average channel mobility may be expressed as

$$\mu_{avg} = \frac{g_d}{\frac{Z}{L} C_G (V_{GS} - V_{ON})} \tag{9}$$

where g_d is the drain conductance, Z is the channel width, L is the channel length, C_G is the gate capacitance per unit area, and V_{GS} is the gate source voltage.[55] Finally, the on/off current ratio measures the strength of the on/off switch. Unsurprisingly, it is defined as the ratio of current passed through the device when it is on to the current passed through the device when it is off.

6.2. Synthesis

Solid state chemistry has developed a myriad of synthetic techniques, but three, pulsed laser deposition, sputtering, and solution processing, dominate TCO synthesis.

6.2.1. Pulsed Laser Deposition

Pulsed laser deposition (PLD) uses a high power pulsed laser in a high vacuum to strike a target of material to be deposited. Upon striking the target, the laser vaporizes a portion of the target into a plasma plume that deposits on a substrate forming a thin film. Although this technique can produce very high quality films over a small area, generating a high vacuum and powering the laser are energy intensive tasks, and it is difficult to use this technique to generate uniform thin films over a large substrate.

6.2.2. Sputtering

In contrast to PLD's usage of a laser to strike a target, sputtering uses high energy particles to accomplish a similar task. A sputtering gas, generally argon, is

ionized by being bombarded with high energy electrons, forming a plasma. Because these particles are ions, they can be directed by an electronic or magnetic field. These ions are directed towards a target material, and when the ions strike the target, they can knock atoms off the surface of the target. These atoms are referred to as sputtered atoms and can form a film when diffusion effects cause them to reach the substrate. Sputtering that uses a magnetic field to direct the path of the sputtering gas is referred to as magnetron sputtering. In order to prevent charge build-up on the target, the sign of the anode/cathode bias may be varied at a high rate (on the order of 10 MHz); this process is referred to as radio frequency (RF) sputtering. On the other hand, if the target is conductive, a direct current may be applied to the target to attract the sputtering gas without the use of a magnetic field; this process is referred to as DC sputtering. RF magnetron sputtering is the most widely used method for the deposition of amorphous oxide films.[8] However, DC sputtering has also been reported to produce high-mobility amorphous oxides in TFTs at substrate temperatures as low as 100°C.[35]

6.2.3. Solution Processing

Solution processing begins with preparing a liquid precursor by dissolving metal cations in either water or an organic solvent. Frequently a stabilizing agent, such as monoethanolamine, is used with organic solvents in order to form a gel; this technique is denoted the sol-gel process. The liquid precursor may be deposited in a number of ways. Inkjet printers may be used to write a precise pattern of the TCO. Alternatively, if a large area needs a uniform layer of a TCO, spin coating may be employed. In this process, the liquid precursor is deposited on a hydrophilic substrate. If the liquid was allowed to evaporate, surface tension would cause the liquid to form droplets, leaving a

non-uniform film once all of the liquid evaporated. Instead, the substrate is spun at high speed (generally 1000-5000 RPM), generating centrifugal force in opposition to the effects of surface tension. This force propels the majority of the solvent off of the substrate, forming a thin gel that subsequently dries into a thin film. In contrast to PLD and sputtering techniques, spin coating does not require high vacuum conditions and theoretically could be scaled for a substrate of any size. An aqueous precursor is preferable to an organic precursor because the organic material is a waste product and must be burned off during annealing, leading to higher processing temperatures and leaving behind pores in the material.

6.3. Characterization Techniques

A variety of characterization techniques were employed for this project. This section gives a basic description of the physical measurements these techniques take, and the way that these measurements are transmitted into relevant information.

6.3.1. Dynamic Light Scattering (DLS)

Dynamic Light Scattering (DLS) is used to determine the size of particles in solution. Monochromatic light, such as light generated by a laser, is shined into a cuvette containing a sample of the solution. The Brownian or random motion of the particles causes a Doppler shift in the wavelength of the incident light. The magnitude of this Doppler shift is a function of the size of the particles in solution, so the particle size may be determined by analyzing the light after it passes through the solution.

6.3.2. Scanning Electron Microscopy (SEM)

A scanning electron microscope shines a focused beam of high energy electrons at a sample and measures the signal of the electron interaction with the sample to generate a two dimensional image of the surface of the sample. Because electrons have much smaller wavelengths than visible light photons, SEM allows imaging at much higher magnifications than optical microscopes.

6.3.3. X-Ray Reflectometry (XRR)

X-ray reflectometry (XRR) directs x-rays at a substrate and measures their reflection. X-rays will reflect off each interface in the sample; taking this project as an example, the x-rays will reflect off of the top of the IGZO surface, off of the interface between the IGZO and the SiO_2 on the surface of the substrate, and finally off of the interface between the SiO_2 and Si within the substrate. The wavelength of the incident x-rays is varied. When the wavelength is an integer multiple of the thickness of a layer, the x-rays reflecting off of the interface at either side of the layer interfere constructively, generating a greater signal. By using computational software to fit a curve to the intensity of the reflected x-rays, the thickness, density, and roughness of each layer can be determined.

6.3.4. Quartz Crystal Microbalance (QCM) Analysis

A quartz crystal microbalance (QCM) measures the frequency of a quartz resonator. This frequency is highly sensitive to mass changes of the resonator, so films are spin coated on top of the quartz and measured after annealing at a variety of

temperatures. The relation between change in frequency and change in mass is given by the Sauerbrey equation

$$\Delta f = -C_f \times \Delta m \qquad (10)$$

where Δf is the frequency change (Hz), C_f is the sensitivity factor (58.3 Hz μg^{-1}cm^2) of the 5MHz AT-cut quartz crystal,[48] and Δm is the mass change per unit area (μg cm^{-2}).

6.3.5. *Infrared (IR) Transmission Spectroscopy*

Infrared (IR) spectroscopy scans a sample with light from the infrared region and the light that the sample transmits is measured. Light of energy corresponding to exciting a feature in the material is absorbed while the remainder is transmitted. Specifically, light from the mid-IR (4000-400 cm^{-1}) is used to determine what functional groups a material contains because light from this region can excite bond stretching and vibration at energy levels characteristic of a particular functional group.

6.3.6. *Transfer Curves and Average Channel Mobility Plots*

In order to assess the average channel mobility and turn-on voltage of a TFT, a constant potential is applied to the gate contact and the source is grounded. This potential is referred to as the gate source voltage, V_{GS}, and is defined as the difference in potential between the gate and the source. Because the source is grounded, it has a potential of zero, so the gate source voltage is simply the potential applied to the gate. The gate dielectric insulates the film, preventing current flow between the gate and either the drain or the source. The gate source voltage is scanned across a large range, here -60 to 60 V, and the current flowing from the drain to the source, so called the drain source current and denoted I_{DS}, is measured as a function of the gate source

voltage. The voltage at which the transistor begins to allow current to flow across from the drain to the source is the turn-on voltage.

7. Bibliography

(1)   Pasquarelli, R. M.; Ginley, D. S.; O'Hayre, R. *Chem. Soc. Rev.* **2011**, *40*, 5406–5441.

(2)   Ellmer, K. *Nat. Photonics* **2012**, *6*, 809–817.

(3)   Fortunato, E.; Ginley, D.; Hosono, H.; Paine, D. C. *MRS Bull.* **2011**, *32*, 242–247.

(4)   Major, S.; Chopra, K. L. *Sol. Energy Mater.* **1988**, *17*, 319–327.

(5)   Ryu, H.; Kang, J.; Han, Y.; Kim, D.; Pak, J. J.; Park, W.-K.; Yang, M.-S. *J. Electron. Mater.* **2003**, *32*, 919–924.

(6)   Sunde, T. O. L.; Garskaite, E.; Otter, B.; Fossheim, H. E.; Sæterli, R.; Holmestad, R.; Einarsrud, M.-A.; Grande, T. *J. Mater. Chem.* **2012**, *22*, 15740.

(7)   Wang, Y.; Liu, S. W.; Sun, X. W.; Zhao, J. L.; Goh, G. K. L.; Vu, Q. V.; Yu, H. Y. *J. Sol-Gel Sci. Technol.* **2010**, *55*, 322–327.

(8)   Kamiya, T.; Hosono, H. *NPG Asia Mater.* **2010**, *2*, 15–22.

(9)   Lee, H. N.; Kyung, J. W.; Kang, S. K.; Kim, D. Y.; Sung, M. C.; Kim, S. J.; Kim, C. N.; Kim, H. G.; Kim, S. T. *IDW06* **2006**, 663–666.

(10)   Jeong, J. K.; Jeong, J. H.; Yang, H. W.; Ahn, T. K.; Kim, M.; Kim, K. S.; Gu, B. S.; Chung, H.-J.; Park, J.-S.; Mo, Y.-G.; Kim, H. D.; Chung, H. K. *J. Soc. Inf. Disp.* **2009**, *17*, 95.

(11)   Son, J.-H.; Ohlin, C. A.; Casey, W. H. *Dalton Trans.* **2012**, *41*, 12674–12677.

(12)   Donaldson, J. D.; Moser, W. *J. Chem. Soc.* **1961**, 1996.

(13)   Casey, W. H. *Chem. Rev.* **2006**, *106*, 1–16.

(14)   Mensinger, Z. L.; Wang, W.; Keszler, D. A.; Johnson, D. W. *Chem. Soc. Rev.* **2012**, *41*, 1019–1030.

(15)   Mensinger, Z. L.; Zakharov, L. N.; Johnson, D. W. *Inorg. Chem.* **2009**, *48*, 3505–3507.

(16)   Donaldson, J. D.; Grimes, S. M.; Johnston, S. R.; Abrahams, I. *J. Chem. Soc. Dalt. Trans.* **1995**, 2273.

(17)   Rather, E.; Gatlin, J.; Nixon, P. G.; Tsukamoto, T.; Kravtsov, V.; Johnson, D. W. *J. Am. Chem. Soc.* **2005**, *127*, 3242–3243.

(18)   Gatlin, J. T.; Mensinger, Z. L.; Zakharov, L. N.; Macinnes, D.; Johnson, D. W. *Inorg. Chem.* **2008**, *47*, 1267–1269.

(19)   Mensinger, Z. L.; Gatlin, J. T.; Meyers, S. T.; Zakharov, L. N.; Keszler, D. A.; Johnson, D. W. *Angew. Chemie* **2008**, *120*, 9626–9628.

(20)   Schweitzer, G. K.; Pesterfield, L. L. *The Aqueous Chemistry of the Elements*; 2010; p. 448.

(21)   Nadarajah, A.; Carnes, M. E.; Kast, M. G.; Johnson, D. W.; Boettcher, S. W. *Chem. Mater.* **2013**, *25*, 4080–4087.

(22)   Wang, W.; Liu, W.; Chang, I.-Y.; Wills, L. a; Zakharov, L. N.; Boettcher, S. W.; Cheong, P. H.-Y.; Fang, C.; Keszler, D. a. *Proc. Natl. Acad. Sci. U. S. A.* **2013**, *13*, 23–27.

(23)   Wang, Y.-L.; Ren, F.; Lim, W.; Norton, D. P.; Pearton, S. J.; Kravchenko, I. I.; Zavada, J. M. *Appl. Phys. Lett.* **2007**, *90*, 232103.

(24)   Choi, C. G.; Seo, S.-J.; Bae, B.-S. *Electrochem. Solid-State Lett.* **2008**, *11*, H7.

(25)   Banger, K. K.; Yamashita, Y.; Mori, K.; Peterson, R. L.; Leedham, T.; Rickard, J.; Sirringhaus, H. *Nat. Mater.* **2011**, *10*, 45–50.

(26)   Chang, Y.-J.; Lee, D.-H.; Herman, G. S.; Chang, C.-H. *Electrochem. Solid-State Lett.* **2007**, *10*, H135.

(27)   Seo, S.-J.; Choi, C. G.; Hwang, Y. H.; Bae, B.-S. *J. Phys. D. Appl. Phys.* **2009**, *42*, 035106.

(28)   Avis, C.; Jang, J. *Electrochem. Solid-State Lett.* **2011**, *14*, J9.

(29)   Nomura, K.; Ohta, H.; Takagi, A.; Kamiya, T.; Hirano, M.; Hosono, H. *Nature* **2004**, *432*, 488–492.

(30)   Kim, G. H.; Shin, H. S.; Ahn, B. Du; Kim, K. H.; Park, W. J.; Kim, H. J. *J. Electrochem. Soc.* **2009**, *156*, H7.

(31)   Park, J. S.; Maeng, W.-J.; Kim, H.-S.; Park, J.-S. *Thin Solid Films* **2012**, *520*, 1679–1693.

(32) Hennek, J. W.; Xia, Y.; Everaerts, K.; Hersam, M. C.; Facchetti, A.; Marks, T. J. *ACS Appl. Mater. Interfaces* **2012**, *4*, 1614–1619.

(33) Zan, H.-W.; Yeh, C.-C.; Meng, H.-F.; Tsai, C.-C.; Chen, L.-H. *Adv. Mater.* **2012**, *24*, 3509–3514.

(34) Kim, G. H.; Du Ahn, B.; Shin, H. S.; Jeong, W. H.; Kim, H. J.; Kim, H. J. *Appl. Phys. Lett.* **2009**, *94*, 233501.

(35) Moon, Y.-K.; Lee, S.; Kim, D.-H.; Lee, D.-H.; Jeong, C.-O.; Park, J.-W. *Jpn. J. Appl. Phys.* **2009**, *48*, 031301.

(36) Tsay, C.-Y.; Huang, T.-T. *Mater. Chem. Phys.* **2013**, *140*, 365–372.

(37) Wang, Y.; Sun, X. W.; Goh, G. K. L.; Demir, H. V.; Yu, H. Y. *IEEE Trans. Electron Devices* **2011**, *58*, 480–485.

(38) Kim, G. H.; Kim, H. S.; Shin, H. S.; Ahn, B. Du; Kim, K. H.; Kim, H. J. *Thin Solid Films* **2009**, *517*, 4007–4010.

(39) Bong, H.; Lee, W. H.; Lee, D. Y.; Kim, B. J.; Cho, J. H.; Cho, K. *Appl. Phys. Lett.* **2010**, *96*, 192115.

(40) Jeong, S.; Ha, Y.-G.; Moon, J.; Facchetti, A.; Marks, T. J. *Adv. Mater.* **2010**, *22*, 1346–1350.

(41) Capello, C.; Fischer, U.; Hungerbühler, K. *Green Chem.* **2007**, *9*, 927.

(42) Meyers, S. T.; Anderson, J. T.; Hung, C. M.; Thompson, J.; Wager, J. F.; Keszler, D. A. *J. Am. Chem. Soc.* **2008**, *130*, 17603–17609.

(43) Jiang, K.; Anderson, J. T.; Hoshino, K.; Li, D.; Wager, J. F.; Keszler, D. A. *Chem. Mater.* **2011**, *23*, 945–952.

(44) Jiang, K.; Zakutayev, A.; Stowers, J.; Anderson, M. D.; Tate, J.; McIntyre, D. H.; Johnson, D. C.; Keszler, D. A. *Solid State Sci.* **2009**, *11*, 1692–1699.

(45) Meyers, S. T.; Anderson, J. T.; Hong, D.; Hung, C. M.; Wager, J. F.; Keszler, D. A. *Chem. Mater.* **2007**, *19*, 4023–4029.

(46) Wang, W.; Wentz, K. M.; Hayes, S. E.; Johnson, D. W.; Keszler, D. A. *Inorg. Chem.* **2011**, *50*, 4683–4685.

(47) Hu, C.; Liu, H.; Qu, J. *Colloids Surfaces A Physicochem. Eng. Asp.* **2005**, *260*, 109–117.

(48)   Trotochaud, L.; Ranney, J. K.; Williams, K. N.; Boettcher, S. W. *J. Am. Chem. Soc.* **2012**, *134*, 17253–17261.

(49)   Zielinski, M. E.; Morris, K. F. *Magn. Reson. Chem.* **2009**, *47*, 53–56.

(50)   Lee, S.-Y.; Park, B.-O. *Thin Solid Films* **2005**, *484*, 184–187.

(51)   Everaerts, K.; Zeng, L.; Hennek, J. W.; Camacho, D. I.; Jariwala, D.; Bedzyk, M. J.; Hersam, M. C.; Marks, T. J. *ACS Appl. Mater. Interfaces* **2013**, *5*, 11884–11893.

(52)   Nomura, K.; Kamiya, T.; Ohta, H.; Hirano, M.; Hosono, H. *Appl. Phys. Lett.* **2008**, *93*, 192107.

(53)   Watanabe, K.; Lee, D.-H.; Sakaguchi, I.; Nomura, K.; Kamiya, T.; Haneda, H.; Hosono, H.; Ohashi, N. *Appl. Phys. Lett.* **2013**, *103*, 201904.

(54)   Hosono, H. *J. Non. Cryst. Solids* **2006**, *352*, 851–858.

(55)   Hong, D.; Yerubandi, G.; Chiang, H. Q.; Spiegelberg, M. C.; Wager, J. F. *Crit. Rev. Solid State Mater. Sci.* **2008**, *33*, 101–132.

(56)   Kamunde-Devonish, M. K.; Jackson, M. N.; Mensinger, Z. L.; Zakharov, L. N.; Johnson, D. W. *Inorg. Chem.* **2014**.

(57)   Nakata, M.; Takechi, K.; Eguchi, T.; Tokumitsu, E.; Yamaguchi, H.; Kaneko, S. *Jpn. J. Appl. Phys.* **2009**, *48*, 081607.

(58)   Hoffmann, R. *Solids and Surfaces: A Chemist's View of Bonding in Extended Structures*; Wiley-VCH, 1989; pp. 1–103.

(59)   Ginley, D. S.; Perkins, J. D. In *Handbook of transparent conductors*; Ginley, D. S., Ed.; Springer US, 2011; pp. 1–25.